Available online at www.sciencedirect.com
ScienceDirect
Bioelectrochemistry 71 (2007) 233–242
Bioelectrochemistry
www.elsevier.com/locate/bioelechem

Electric field-mediated transport of plasmid DNA in tumor interstitium in vivo

Joshua W. Henshaw, David A. Zaharoff [1], Brian J. Mossop, Fan Yuan *

Department of Biomedical Engineering, Duke University, 136 Hudson Hall, Durham, NC 27708, USA

Received 10 November 2006; received in revised form 7 July 2007; accepted 18 July 2007
Available online 1 August 2007

Abstract

Local pulsed electric field application is a method for improving non-viral gene delivery. Mechanisms of the improvement include electroporation and electrophoresis. To understand how electrophoresis affects pDNA delivery in vivo, we quantified the magnitude of electric field-induced interstitial transport of pDNA in 4T1 and B16.F10 tumors implanted in mouse dorsal skin-fold chambers. Four different electric pulse sequences were used in this study, each consisted of 10 identical pulses that were 100 or 400 V/cm in strength and 20 or 50 ms in duration. The interval between consecutive pulses was 1 s. The largest distance of transport was obtained with the 400 V/cm and 50 ms pulse, and was 0.23 and 0.22 μm/pulse in 4T1 and B16.F10 tumors, respectively. There were no significant differences in transport distances between 4T1 and B16.F10 tumors. Results from in vivo mapping and numerical simulations revealed an approximately uniform intratumoral electric field that was predominantly in the direction of the applied field. The data in the study suggested that interstitial transport of pDNA induced by a sequence of ten electric pulses was ineffective for macroscopic delivery of genes in tumors. However, the induced transport was more efficient than passive diffusion.

Keywords: In vivo DNA electrophoresis; Interstitial transport; Non-viral gene therapy; DNA electrotransfer; Electric field-mediated gene delivery

1. Introduction

The efficacy of non-viral gene therapy is limited by poor delivery of therapeutic genes into the nucleus of target cells. A rate-limiting physiological barrier to gene delivery is the interstitial space. In tumor interstitium, convection is negligible due to a uniformly elevated interstitial fluid pressure [1], leaving gene delivery through the extracellular matrix (ECM) to rely on passive diffusion [2]. Unfortunately, diffusion is also inefficient for larger therapeutics in tumors [3], and can be considered as a negligible transport mechanism for therapeutics the size of a typical plasmid DNA (pDNA). The limited interstitial transport implies that only the pDNA molecules localized within a very thin layer outside the cell membrane have the potential to enter the cell and elicit successful transgene expression. Increasing pDNA interstitial transport may significantly increase the thickness of this layer in vivo, and therefore the transfection efficiency of pDNA. One strategy to improve the interstitial transport is to locally apply a pulsed electric field to push exogenous genes in tumors.

Electric field-mediated gene delivery has been investigated extensively both in vitro [4–7] and in vivo [8–21]. Mechanisms of the delivery include cell membrane electroporation and DNA electrophoresis. Electroporation has been studied extensively in vitro [22–30]. The process is characterized by an increased permeability of the cell membrane to traditionally non-permeant molecules, caused by the presence of an external, pulsed electric field. The permeability increase is thought to occur due to the formation of transient, hydrophilic pores in the cell membrane in response to an above threshold transmembrane potential [31]. These pores allow cellular uptake of small molecules primarily by passive diffusion. For larger molecules such as pDNA, mechanisms of the uptake remain unclear [32], however studies have shown that the process involves DNA absorption to the cell envelope prior to transport across the membrane [33]. Regardless of the uptake mechanisms, the pDNA must be within a critical distance from the cell membrane in order to be taken up by the

* Corresponding author. Tel.: +1 919 660 5411; fax: +1 919 684 4488.
E-mail address: fyuan@duke.edu (F. Yuan).
[1] Present address: Laboratory of Tumor Immunology and Biology, National Cancer Institute (NIH), Bethesda, MD 20892, USA.

1567-5394/$ - see front matter © 2007 Elsevier B.V. All rights reserved.
doi:10.1016/j.bioelechem.2007.07.005

permeabilized cell. This distance may be increased through in vivo electrophoresis in the presence of an external, pulsed electric field.

Despite its potential significance, the in vivo electrophoresis component of electric field-mediated gene delivery is only the focus of a few studies in the literature [34–38]. The significance of the electrophoretic component has been demonstrated in vivo in muscle by studying the transfection levels obtained using a combination of low voltage, non-porating pulses with long duration (LV), and high voltage, porating pulses with short duration (HV). Bureau et al. reported high levels of transgene expression following a pulse sequence consisting of a single HV (800 V/cm, 0.1 ms), followed by four LVs (80 V/cm, 83 ms) [34]. Satkauskas et al. later demonstrated that the HV resulted in electropermeabilization and the LVs resulted in pDNA electrophoresis [35]. A recent study by Satkauskas et al. revealed that the LVs played an important role in determining the levels of transgene expression following a prerequisite HV [36]. These studies demonstrate the significant effects the electrophoretic component has on in vivo cell transfection following the initial pore formation. However, these studies fail to distinguish between the potential roles of electrophoresis in increasing interstitial transport versus facilitating cellular uptake. Furthermore, it is still unclear how far and how fast the pDNA can move during electrophoresis.

In this study, we investigated the ability of an applied pulsed electric field to overcome the interstitial barrier by quantifying the magnitude of in vivo electric field-induced transport of pDNA in tumor interstitium. Zaharoff et al. have previously reported pDNA electromobility ex vivo in tumor interstitium [37], as well as pDNA electromobility in agarose tissue phantoms [38]. Here, we used a similar technique to quantify interstitial transport of pDNA in vivo in two types of tumors (4T1 and B16.F10) grown in mouse dorsal skin-fold chambers (DSCs), and correlated the observed electrophoretic movement with the tissue collagen content as has been observed in previous studies [37,39]. Furthermore, we experimentally mapped and numerically simulated the in vivo distribution of electric potential in tumors. The potential distribution determines the local field strength that is the driving force for electrophoresis in tumor interstitium.

2. Materials and methods

2.1. Tumor model

4T1 (a murine mammary carcinoma) and B16.F10 (a metastatic subline of B16 murine melanoma) cells were cultured in DMEM supplemented with 10% fetal bovine serum, 100 U/ml streptomycin, and 100 U/ml penicillin at 37 °C, 95% air and 5% carbon dioxide. Cells were harvested from flasks with 0.25% trypsin/EDTA and rinsed with DMEM then PBS. Cells were centrifuged for 2 min at 176 g and re-suspended in PBS to a final concentration of 5×10^7 cells/ml. Fluorescently labeled, electrically neutral, yellow-green latex microspheres with a diameter of 1.0 μm (YG-MS, Polysciences, Inc., Warrington, PA, USA) were added to the cell suspension to be used as a tissue marker during image analysis.

Female BALB/C and C57BL/6 mice (18–24 g, Charles River, Raleigh, NC, USA) were used as hosts for 4T1 and B16.F10 tumors, respectively. DSCs were implanted in mice anesthetized with an i.p. injection of 80 mg ketamine and 10 mg xylazine per kg body weight. 10 μl of cell suspension ($\sim5\times10^5$ cells) were injected into the fascia layer at the center of the DSC, and then the DSC was sealed with a glass coverslip. Tumors were allowed to grow 5–6 days and 7–10 days for 4T1 and B16.F10, respectively.

2.2. pDNA administration

Once the tumors had reached 3–4 mm in diameter, the mice were anesthetized and the coverslip was removed from the DSC. Approximately 1 μg of rhodamine-labeled plasmid DNA (Rho-pDNA, 5.1 kb, Gene Therapy Systems, San Diego, CA, USA) was injected into the center of the tumor using a microinjection system consisting of a TransferMan NK micromanipulator and a CellTram Vario oil pump (Eppendorf, Westbury, NY, USA) mounted on an Axioskop 2 Plus upright microscope (Zeiss, Thornwood, NY, USA). This method allowed precise control over the location and amount of pDNA delivered while limiting damages to tumor tissue and vasculature. The tissue was washed thoroughly with PBS, and then the DSC was resealed with a sterile glass coverslip.

2.3. Electric field application

Anesthetized mice were secured on a custom designed microscope stage on a Model 510 confocal microscope (Zeiss). A localized electric field was applied using two stainless steel, parallel plate electrodes on the skin side of the DSC (see Fig. 1). An electric potential difference was supplied by an ECM 830 electro square porator (BTX, San Diego, CA, USA). Pulsed electric fields examined in this study consisted of 10 identical square voltage pulses with a magnitude of 100 or 400 V/cm and a duration of 20 or 50 ms. The interval between consecutive pulses was 1 s.

2.4. Image acquisition

Fluorescence images of the Rho-pDNA and YG-MS were acquired using a 40× objective before and immediately following the application of an entire 10-pulse sequence. The area of the image was away from the needle track to ensure the area of the tissue imaged was not damaged during plasmid administration. The one-dimensional resolution of the acquired images was 0.44 μm/pixel. Images for control groups were taken with a 10 s delay between image acquisitions during which no electric field was applied.

2.5. Image analysis

A cross-correlation analysis was performed on the fluorescence images taken before and following application of the pulsed electric field. The analysis was performed independently on channel 1 and channel 2 to determine the linear drift displacement, averaged over a field of view, of Rho-pDNA ($\vec{D}_{\mathrm{pDNA}}$) and YG-MS ($\vec{D}_{\mathrm{MS}}$) respectively. Details of the analysis are as follows. Pre- and post-pulse sequence images are represented by $p(x, y)$ and $q(x, y)$, respectively, where x and y are the indices of pixels in each image. If image $p(x, y)$ is fixed and image $q(x, y)$ is shifted

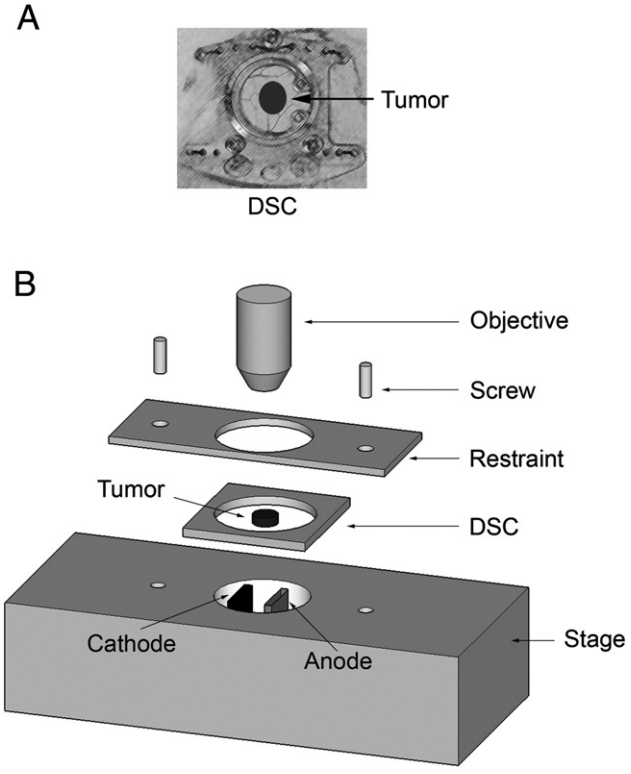

Fig. 1. Diagram of the experimental setup used in this study. A DSC with tumor is shown in Panel A. Panel B shows how a DSC was secured to a stage of confocal microscope. The electric field was applied to the tumor through the parallel-plate electrodes in contact with the skin side of the DSC while the objective of microscope had access to the tumor on the window side of the DSC. An illustration of a mouse implanted with a DSC can be found in [59].

by i and j pixels in x and y directions, respectively, the normalized cross-correlation coefficient of the two images is given by

$$r_{ij} = \frac{\sum_x \sum_y [p(x,y) - p_{\text{mean}}][q(x+i, y+j) - q_{\text{mean}}]}{\sigma_p \sigma_q} \quad (1)$$

where p_{mean} and q_{mean} are the mean intensities in the images $p(x, y)$ and $q(x+i, y+j)$ respectively, and σ_p and σ_q are defined as follows.

$$\sigma_p = \sqrt{\sum_x \sum_y [p(x,y) - p_{\text{mean}}]^2} \quad (2)$$

$$\sigma_q = \sqrt{\sum_x \sum_y [q(x+i, y+j) - q_{\text{mean}}]^2}. \quad (3)$$

The summations above include only overlapping pixels between p and q. $\vec{D}_{\text{pDNA}}$ and $\vec{D}_{\text{MS}}$ were then determined by the vector (i_m, j_m),

$$\vec{D} = \alpha(i_m, j_m) \quad (4)$$

where i_m and j_m were the indices at which the correlation coefficient, r_{ij}, reached a maximal value, and α is a conversion factor between distance in pixels and distance in microns ($\alpha = 0.44$ μm/pixel).

Due to their size and neutral charge, YG-MSs were assumed to have remained locked in place with respect to surrounding tissue and were therefore used as markers for tissue movement. The electric field-induced pDNA movement, defined as the pDNA displacement relative to the tumor tissue, was determined on a per pulse basis by,

$$d_{\text{p}} = \frac{|\vec{D}_{\text{pDNA}} - \vec{D}_{\text{MS}}|}{N} \quad (5)$$

where d_{p} is the electric field-induced pDNA movement per pulse and N is the number pulses for the applied field ($N = 10$ for all pulsing conditions used in this study).

The in vivo electric field-induced pDNA movement was determined in seven 4T1 and seven B16.F10 tumors for each of the four pulsing conditions examined in this study. The average pDNA movement for each pulse condition is reported with error bars representing the standard deviations of the data.

2.6. In vivo pDNA electromobility

The efficiencies of the different electric fields used in this study to induce pDNA movement were compared by calculating the pDNA electromobility for each of the pulse conditions. The pDNA electromobility, μ, was determined from Eq. (6),

$$v = \mu E_t = \frac{d_{\text{p}}}{t_{\text{p}}} \quad (6)$$

where v is the magnitude of the drift velocity of pDNA, E_t is the magnitude of the intratumoral electric field determined by the linear regression analysis of the experimentally mapped electric potential distribution (see the Materials and method section on *intratumoral potential distribution*), and t_{p} is the pulse duration.

2.7. Collagen assay

A hydroxyproline assay was performed to determine the average collagen content in tumors grown in DSCs. 4T1 and B16.F10 tumors (3–4 mm in diameter) were excised from animals and incubated in 1.0 ml digesting buffer (126 μg/ml papain in 0.1 M $NaHPO_4$, 5.0 mM EDTA, and 5.0 mM L-cysteine-HCL, pH 6.0) for 20 h at 60 °C. 100 μl of each papain digest were then hydrolysed in 900 μl 6 N HCl for 20 h at 115 °C. Samples were brought to room temperature and two drops of 0.02% methyl red indicator were added. Sample solutions were neutralized with 2.5 M NaOH, followed by 0.5 M HCl and, finally, 0.5 M NaOH. The final volume, following titration, of each sample was determined. 1.0 ml chloramines T solution (705 mg chloramine T in 40 ml pH 6.0 buffer and 5 ml isopropanol) was then added to 1.0 ml of each sample and allowed to stand for 20 min at room temperature. The pH 6.0 buffer consisted of 5.0 g citric acid monohydrate, 12.0 g sodium acetate trihydrate, 3.4 g NaOH, and 1.2 ml glacial acetic acid, which were brought to 100 ml with distilled water. 1.0 ml pDAB solution (4.0 g *p*-dimethylaminobenzaldehyde (pDAB) in 16.0 ml isopropanol and 7.0 ml perchloric acid (60%)) was added and samples were incubated for 20 min at 60 °C. Samples were

cooled in a room temperature water bath for 5 min. The absorbance of the solutions at 557 nm was recorded within 1 h following cooling. A standard hydroxyproline curve was established by dissolving 0–5 μg hydroxyproline in 1 ml deionized water and repeating the above procedure from the step of chloramines T addition. Hydroxyproline is an amino acid derivative exclusive to collagen and accounts for approximately 12.5% of the total collagen mass [40]. The average collagen content was determined for three 4T1 and three B16.F10 tumors.

2.8. Collagen histology

Histological analysis was performed on tumor sections to visualize the collagen content and distribution. 4T1 and B16.F10 tumors were excised from the DSCs in BALB/C and C57BL/6 mice, respectively, and fixed in 10% formalin for 24 h. Tumors were then embedded in paraffin, sectioned at 5 μm, and stained with a Masson trichrome solution.

2.9. Intratumoral potential distribution

The intratumoral electric potential distribution determines the electric field, which is the driving force for in vivo electrophoresis. The local electric fields within 4T1 and B16.F10 tumors were mapped with a microelectrode array. The DSC coverslip was removed from anesthetized mice secured on the custom microscope stage. A 5 × 5 array of microelectrodes (Bionic Technologies Inc., Salt Lake City, UT, USA) was placed at the center of the tumor, depressed slightly into the tissue, and held in place with clay. This placement coincided with the approximate location at which pDNA images were taken. The electrode array consisted of 25 glass enclosed, platinum electrodes. Total electrode length was 1 mm, with a 50 μm bare platinum tip, 2.0 μm in diameter. Inter-electrode spacing was 400 μm. The potential at each electrode was recorded during the application of a 100 or 400 V/cm, 20 ms pulse using an Enhancer 400 oscilloscope (BTX). Readings at each electrode were taken in triplicate and averaged. A linear decrease in potential as a function of pulse number was observed during the course of these measurements. To compensate for this decrease in potential, linear regression analysis was performed on the three readings at each potential and the resulting slopes of these plots were averaged over the 25 electrodes. This correction factor was then applied to each potential reading as a function of pulse number. The potential data at each location used in the isopotential plots was the average of the three corrected readings. The potential distribution was determined in three 4T1 and three B16.F10 tumors.

The magnitude of the electric field within a tumor was determined by linear regression analysis of the potential distribution recorded by the array of microelectrodes. If the distribution is uniform and unidirectional, the potential, Φ, can be fit by the function,

$$\Phi = ax + by \tag{7}$$

where x and y are the known coordinates of the recording electrodes and a and b are constants. Once the values of a and b were determined numerically through linear regression analysis, the magnitude of the electric field was calculated as the magnitude of the potential gradient.

2.10. Numerically simulated potential distribution

A commercially available finite element software (Comsol Multiphysics 3.2, COMSOL, Inc., Burlington, MA) was used to determine the electric potential distribution as a function of depth within the tumor. The concern here was possible variation in the field strength in the experimental setup used in this study. A two-dimensional volume conductor model of the cross-section of the DSC was used, based on the assumed symmetry of the setup. The geometry of the model was determined through experimental measurements of a representative DSC model used in this study. Since current sources existed only at the skin-electrode interfaces, the potential distribution in the DSC was governed by the Laplace equation,

$$\nabla \cdot \vec{J} = -\sigma \nabla^2 \Phi = 0 \tag{8}$$

where $\vec{J}$ is the current density, σ is the conductivity of the conducting medium through which the current is flowing, and Φ is the electric potential. There were no currents across external surfaces, i.e., the no-flux boundary condition was satisfied on these boundaries,

$$\vec{n} \cdot \vec{J} = 0 \tag{9}$$

where $\vec{n}$ is the unit vector in the normal direction of the boundary. Across all internal interfaces in the DSC, the current was continuous, i.e., the continuous boundary condition was satisfied,

$$\vec{n} \cdot (\vec{J}_1 - \vec{J}_2) = 0 \tag{10}$$

except at the skin-anode and skin-cathode interfaces where the potentials were set at 50 V and 0 V, respectively. $\vec{J}_1$ and $\vec{J}_2$ are the current vectors on different sides of the interface that was in the direction of $\vec{n}$. The conductivities of the glass coverslip and electrodes were assumed to be 10^{-12} and 10^{9} S/m respectively. The conductivities used for the skin, connective tissue, and tumor tissue were 0.2, 0.04, and 0.4 S/m, respectively [41].

2.11. Statistical analysis

The magnitudes of pDNA movement in all experimental groups were tested against zero, using a 1-sample sign test with a test mean of zero. Differences in data between any two experimental groups were compared using the Mann–Whitney test. All statistical calculations were performed using Minitab statistical software (Minitab Inc, State College, PA, USA).

3. Results

3.1. In vivo Imaging of pDNA and tissue marker

Mouse DSC tumor models allowed noninvasive access to tumor interstitium with fluorescence confocal microscopy. The

DSC was secured on a confocal microscope stage that allowed simultaneous electric field application and image acquisition. A diagram of the experimental setup is shown in Fig. 1. Images of microinjected Rho-pDNA and YG-MS within tumor interstitium in the DSCs were obtained using a 40× water immersion objective. The microscope was set to a multichannel configuration, with channel 1 capturing the Rho-pDNA signal, and channel 2 capturing the YG-MS signal. The images were taken in a line-switching mode to prevent cross talk between the channels. A representative image is shown in Fig. 2.

3.2. In vivo electric field-induced pDNA movement

The electrophoretic movement of pDNA in pulsed electric fields was determined by comparing confocal images taken immediately before and immediately after pulse application. The distance of electric field-induced pDNA movement per pulse, d_p, was determined for a set of four pulsing conditions in both 4T1 and B16.F10 tumors (Fig. 3). Under each condition, 10 identical square wave pulses were applied sequentially to tumors, with the time interval between pulses being 1 s. The strength and duration of pulses were 100 or 400 V/cm and 20 or 50 ms, respectively.

The magnitude of pDNA movement observed without the application of a pulsed electric field was not significantly different from zero in both 4T1 and B16.F10 tumors ($P=0.50$ for both tumors). The magnitude of pDNA movement was significantly greater than zero for each applied field in both tumor types ($P<0.05$ for all groups). The distances of pDNA movement in 4T1 tumors subjected to a 100 V/cm pulsed field were 2.4×10^{-2} μm and 3.3×10^{-2} μm for pulse duration of 20 and 50 ms, respectively. The distances were increased to 9.51×10^{-2} μm and 2.27×10^{-1} μm, respectively, when the field strength was increased to 400 V/cm. In B16.F10 tumors, the distances of pDNA movement subjected to a 100 V/cm pulsed field were 4.52×10^{-2} and 5.05×10^{-2} μm for pulse duration of 20 and 50 ms, respectively. The distances were increased to 9.93×10^{-2} μm and 2.23×10^{-1} μm, respectively, when the field strength was increased to 400 V/cm.

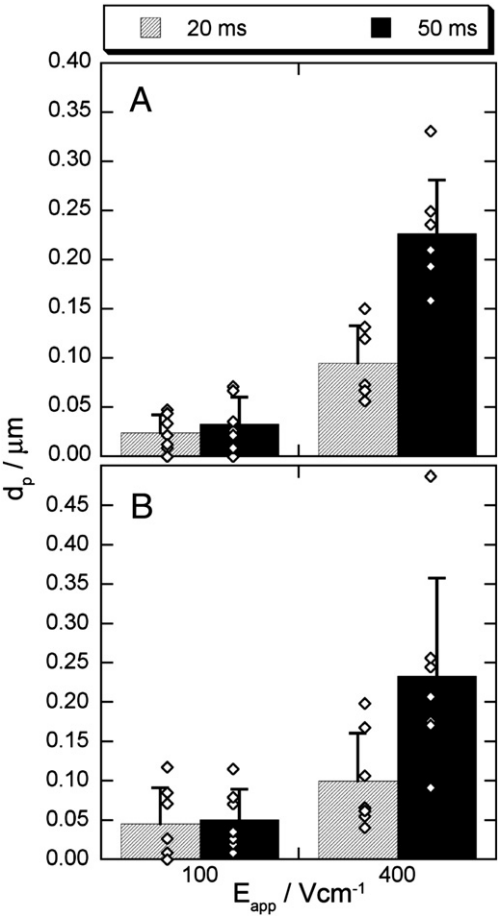

Fig. 3. Mean values of net pDNA movement per pulse, d_p, in 4T1 (A) and B16.F10 (B) tumor interstitium with an applied electric field that consisted of 10 identical pulses with 100 or 400 V/cm in magnitude and 20 or 50 ms in duration. The interval between consecutive pulses was 1 s. The symbols represent individual data points and the error bars represent the standard deviations of the data ($n=7$).

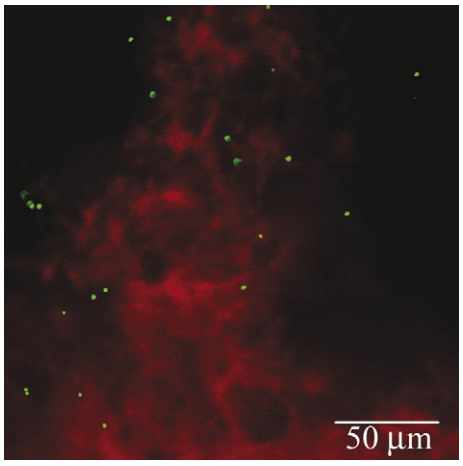

Fig. 2. A representative confocal image of Rho-pDNA (red) and YG-MS (green) in tumor tissues in the DSC in vivo. The image was acquired in a multichannel configuration of the confocal microscope, using a 40× water immersion objective. (For interpretation of the references to colour in this figure legend, the reader is referred to the web version of this article.)

The differences between the data from different groups were compared statistically and the *P*-values are shown in Table 1. With a 100 V/cm field, increasing the pulse duration from 20 to 50 ms did not result in a significant increase in electrophoretic movement of pDNA in either 4T1 or B16.F10 tumor. However, with a 400 V/cm field, the electrophoretic movement was significantly increased when increasing the pulse duration from 20 to 50 ms in both tumor types. If the pulse duration was fixed at 20 ms, increasing the field strength from 100 to 400 V/cm resulted in a significant increase in pDNA electrophoretic movement in 4T1 tumors, but not in B16.F10 tumors. With the 50 ms pulses, increasing the field strength from 100 to 400 V/cm did result in a significant increase in pDNA electrophoretic movement in both 4T1 and B16.F10 tumors. Finally, the distances of pDNA movement were not statistically different between 4T1 and B16.F10 tumors under any pulsing conditions investigated.

Table 1
P-values in statistical comparisons of electric field-induced interstitial transport distances

			4T1				*B16.F10*			
			100 V/cm		400 V/cm		100 V/cm		400 V/cm	
			20 ms	50 ms	20 ms	50 ms	20 ms	50 ms	20 ms	50 ms
4T1	100 V/cm	20 ms	1.000							
		50 ms	0.655	1.000						
	400 V/cm	20 ms	0.002	0.015	1.000					
		50 ms	0.002	0.002	0.002	1.000				
B16.F10	100 V/cm	20 ms	0.655	0.748	0.097	0.002	1.000			
		50 ms	0.225	0.443	0.097	0.002	0.749	1.000		
	400 V/cm	20 ms	0.005	0.041	0.609	0.007	0.160	0.160	1.000	
		50 ms	0.002	0.002	0.007	0.798	0.003	0.003	0.015	1.000

The *P*-values were determined by Mann–Whitney test. The difference for each comparison of the data shown in Fig. 2 was statistically significant if $P<0.050$.

3.3. In vivo pDNA electromobility

To further compare the magnitudes of pDNA movement within the tumor under different pulsing conditions, the electromobility of the pDNA was calculated and the results are shown in Fig. 4. The difference in electromobility between any two groups was statistically insignificant ($P>0.05$).

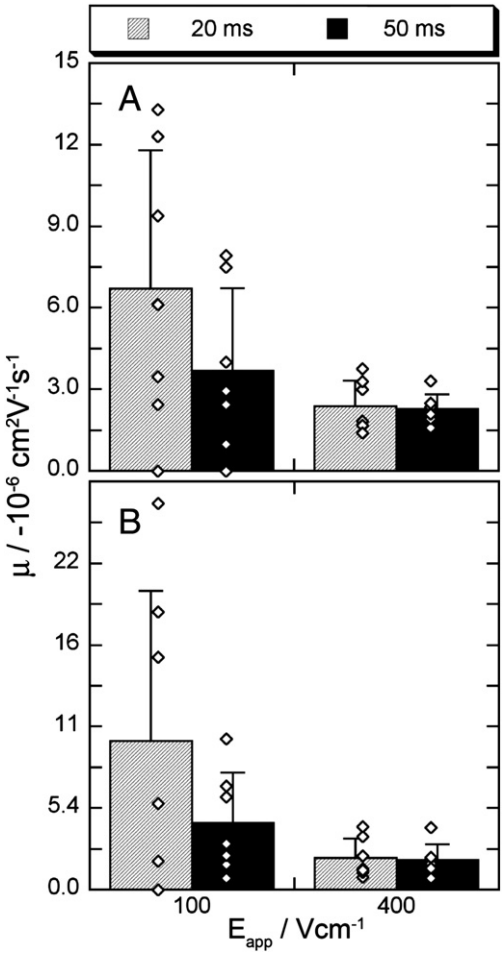

Fig. 4. Mean values of electromobility, μ, of pDNA in 4T1 (A) and B16.F10 (B) tumor interstitium with an applied electric field that consisted of 10 identical pulses that were 100 or 400 V/cm in magnitude, E_{app}, and 20 or 50 ms in duration. The interval between consecutive pulses was 1 s. Electromobility was calculated using the measured pDNA movement shown in Fig. 3 and intratumoral electric field determined in a separate experiment. Differences in the electromobility between any two groups were not statistically significant ($P>0.05$). Symbols represent individual data points and error bars represent the standard deviations of the data ($n=7$).

3.4. Collagen content

Zaharoff et al. have previously demonstrated that pDNA electrophoretic movement in excised tumor tissues correlates with the collagen content of the tissue [37]. To determine if this was also the case in vivo, a hydroxyproline assay was performed to quantify the collagen content in 4T1 and B16.F10 tumors. The collagen contents observed in three 4T1 tumors were 4.63 μg, 4.32 μg, and 4.98 μg (mean 4.64 μg) per

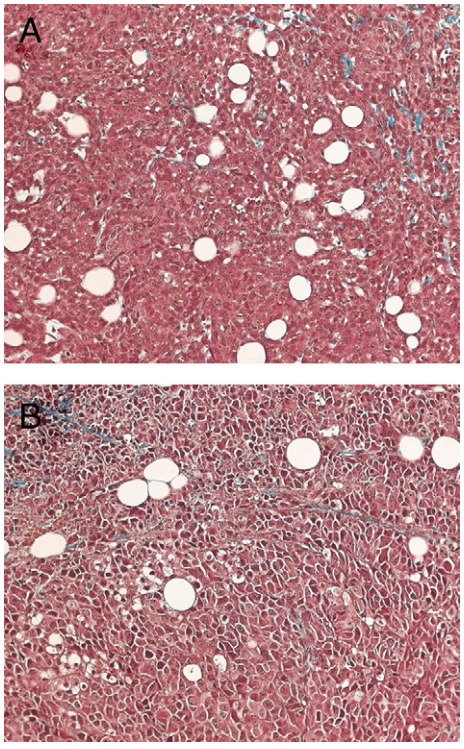

Fig. 5. Masson trichrome staining of 4T1 (A) and B16.F10 (B) tumor sections (5 μm in thickness). Cytoplasm and nuclei are stained pink and collagen is stained blue. (For interpretation of the references to colour in this figure legend, the reader is referred to the web version of this article.)

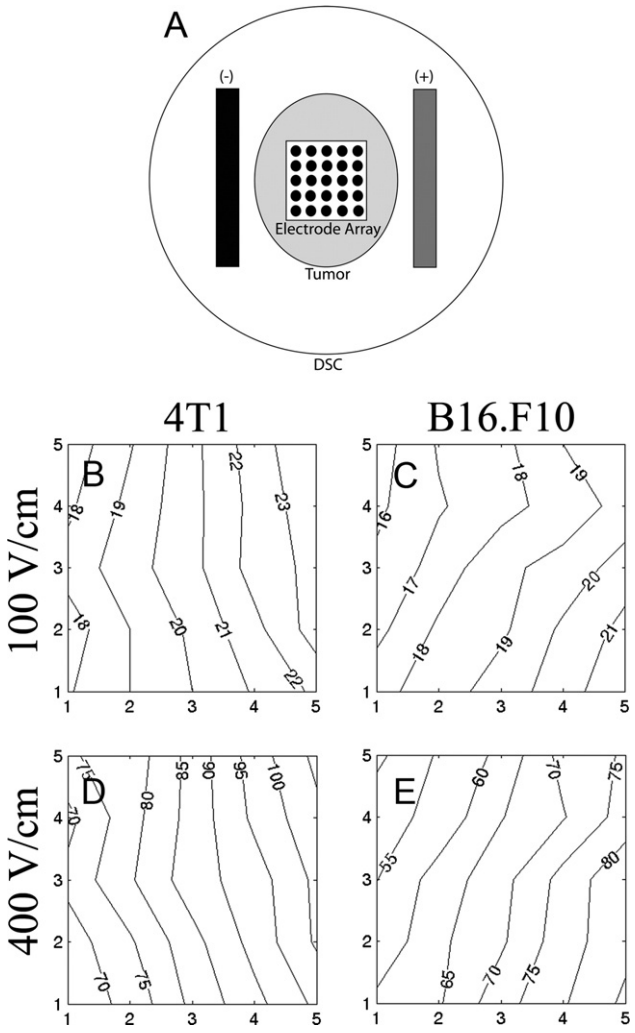

Fig. 6. (A) A schematic of electrode array placement for recording of intratumoral potential distribution. Other panels in the figure show isopotential plots in 4T1 (B, D) and B16.F10 (C, E) tumors during the application of a 100 V/cm (B, C) or 400 V/cm (D, E) pulse with 20 ms in duration. The label on each isopotential plot indicates the value of electric potential. The labels of the horizontal and vertical axes represent the coordinates of the recording electrodes on the 5×5 electrode array. Center-to-center spacing of adjacent recording electrodes was 400 μm.

mg of wet tissue, respectively. The data in three B16.F10 tumors were 3.35 μg, 3.44 μg, and 5.98 μg (mean=4.26 μg) per mg of wet tissue, respectively. The difference in the collagen content between 4T1 and B16.F10 tumors grown in DSCs was not statistically significant ($P=0.705$).

Histological analysis was also performed on 4T1 and B16.F10 tumor sections excised from DSCs. Masson trichrome staining of the 5-μm sections revealed similar levels of collagen content in 4T1 and B16.F10 tumors (Fig. 5). In addition, the histological images showed a heterogeneous distribution of collagen within individual sections. The heterogeneity might contribute to the variations in the magnitude of electric field-induced pDNA movement indicated by the scattering of data points shown in Fig. 3.

3.5. In vivo electric potential distribution

The intratumoral electric potential distribution, and the resulting electric field, were mapped in vivo using a 5×5 microelectrode array (see Fig. 6). The array, commonly referred to as a Utah array, was depressed slightly into the center of a tumor. The potentials at each of the 25 electrodes were recorded sequentially when 25 identical pulses with the strength of 100 or 400 V/cm and duration of 20 ms were applied. The measurements were performed three times at each electrode and the average results are reported here. Representative potential distributions within both 4T1 and B16.F10 tumors are shown as isopotential plots in Fig. 6. The intratumoral electric fields were approximately uniform in both tumor types. The slight nonlinearities in the isopotential plots should not drastically affect the magnitude of driving force, i.e., the magnitude of electric field, for the electrophoretic movement observed in this study.

The magnitudes of the electric field were determined through a linear regression analysis of the isopotential plots obtained with the Utah array. They were 17.9 V/cm and 200 V/cm in 4T1 tumors for the 100 V/cm and 400 V/cm applied fields, respectively. The magnitudes in the B16.F10 tumors for the same applied fields were 23.0 and 237 V/cm, respectively.

The electric potential distribution in the tumor implanted in a DSC was also simulated numerically using a finite element method. The isopotential plot in a cross section of the DSC, which was a plane perpendicular to the skin and the parallel-plate electrodes, is shown in Fig. 7. The plot suggested that the electric field near the center of the tumor, where the pDNA electrophoretic movement was measured, was approximately uniform and predominantly in the direction of applied field.

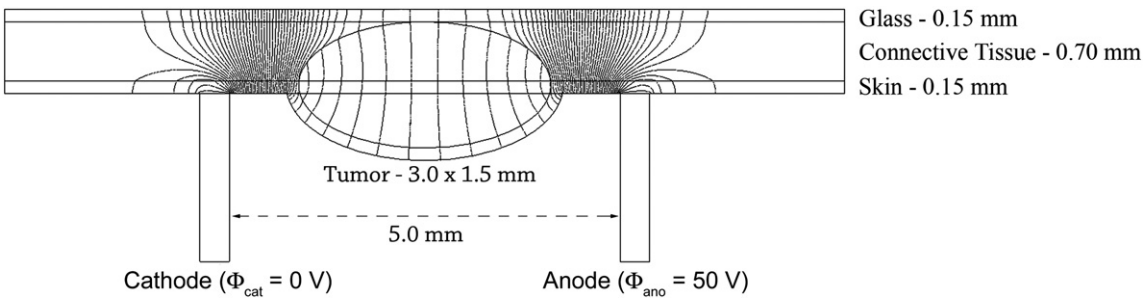

Fig. 7. Isopotential plot in a DSC cross-section using the data from the numerical simulations. The strength of the applied field was 100 V/cm. The potential difference between adjacent plots is 0.5 V.

4. Discussion

We successfully adapted the experimental technique, developed previously for ex vivo pDNA mobility measurement, to quantify in vivo electrophoresis of pDNA in electric field-mediated gene delivery in tumor interstitium. The technique was based on the DSC mouse model that allowed noninvasive access to living tumor interstitium with fluorescence confocal microscopy, and the cross-correlation analysis that allowed quantification of average pDNA displacement within a field of view.

Electrical parameters for in vivo DNA electrotransfer have yet to be homogenized in the literature. In particular, pulse duration may vary from less than 100 μs up to 50 ms and pulse strength may vary from 10 V/cm to up to 2.0 kV/cm. Both the strength and the duration of electric pulses can affect the scale of electrophoretic movement of pDNA. It is plausible that increasing these parameters can enhance pDNA electrophoretic movement. Unfortunately, increasing the energy of the applied pulses also increases their adverse effects on tissues. Therefore, the higher energy pulses, which may result in an irreversible cell membrane modification [42,43], are unlikely to be suitable for clinical use.

The pulse durations of 20 and 50 ms used in this study, which represent the longer duration pulses used in the literature, were considered to result in the greatest degree of electric field-induced pDNA mobility [35]. On the other hand, the in vivo mobility data reported in this study showed that electric fields applied transcutaneously with parallel-plate electrodes were only effective in driving pDNA over distances less than 0.25 μm per pulse, or 2.5 μm per 10-pulse sequence. The magnitude of this movement is insignificant in terms of macroscopic transport within a tumor since it accounts for only one quarter of the diameter of a single cell (~10 μm). This observation suggests that electric fields are not a viable option for enhancing the macroscopic distribution of pDNA within solid tumors. Other techniques, such as intratumoral infusion [44–46], are likely to be better choices for improving pDNA distribution within a tumor.

While the electrophoretic component of electric field-mediated gene delivery may not play a significant role in macroscopic pDNA movement, it may still have significant contributions to enhancing gene delivery in vivo. Results from this study showed that in the absence of an applied field, there was no detectable interstitial transport of pDNA. The distance of pDNA movement was statistically greater than zero only if a pulsed field was applied to tumors. This observation confirmed a notion that DNA electrophoresis was several orders of magnitude faster than passive diffusion [37,38]. As a result, the interstitial electrophoresis could effectively push more pDNA molecules towards the transient pores in the plasma membrane of cells. While mechanisms of cellular uptake of pDNA are still not fully understood [47–50], the increase in extracellular transport of pDNA towards the pores could contribute to the increased levels of transgene expression observed in previous studies [34–36].

Previous reports have shown that electric fields are effective in driving the movement of pDNA over a greater distance in tissue phantoms composed of agarose gels [38]. Agarose gels are considered as accurate phantoms for tissue interstitium, as the fibrous network formed by agarose during solidification is structurally similar to the extracellular matrix (ECM) in tissue interstitium. The discrepancies between the magnitudes of electrophoretic movement reported in the Ref. [38] and those reported here may be attributed to differences in fiber spacings and local electric fields between the phantoms and tumor tissues. We have demonstrated that electric fields in the phantoms are significantly higher than those in tumor tissues when exposed to the same pulsed electric fields [51]. Furthermore, the spacings in agarose gels are likely to be significantly larger than those in tumor ECM [3,38].

Zaharoff et al. have previously demonstrated that the electrophoretic mobility of pDNA in 4T1 tumors, when determined ex vivo, is significantly different from that in B16.F10 tumors [37]. The in vivo results obtained in this study showed no significant difference between the two tumors. Nevertheless, the levels of electrophoretic mobility in both studies correlated with the collagen content of the tumor. These observations were consistent with that of the diffusion coefficient of macromolecules in tumors, which also correlates with the collagen content [39,52], suggesting that collagen is one of the main barriers for interstitial transport of macromolecules.

The differences in the collagen content between the ex vivo and the in vivo studies mentioned above might be attributed to the different locations of tumor growth. Tumors used in the ex vivo experiments were harvested from the hind leg, while tumors in this study were from the DSC. Previous studies have shown that tumor composition can vary with the site of implantation [53]. In addition, the differences in the collagen content might be due to different stages of tumor growth. In the ex vivo study, tumors were excised when they reached ~10 mm in diameter. In this study, tumors were used when they were 3–4 mm in diameter.

The local electric field was mapped in vivo in mouse DSCs in this study. The results demonstrated that the electric fields, which were the driving force for pDNA movement, were approximately uniform in the central region of tumors where the electrophoretic mobility was measured. The slight nonlinearity observed in the isopotential plots in both tumors shown in Fig. 6 might be attributed to inhomogeneities in tissue structures, as shown in histological examinations (see Fig. 5). A common trend observed in the isopotential plots shown in Fig. 6 was that the nonlinearity was a function of the tissue structure but not the magnitude of the applied field. Results from the numerical simulations also demonstrated little variation in the electric field as a function of depth in the central region of the tumor (see Fig. 7). The intratumoral electric field will not be uniform if the external electric field is applied through needle electrodes [54,55].

The intratumoral electric fields mapped in the central region were approximately 20% of the applied field at 100 V/cm in both tumors and increased to approximately 55% of the applied field at 400 V/cm. The increase was mainly due to electric field-induced reduction in the total electrical resistance of skin and electrode-tissue interface [51]. To further increase the electric field in tumors, one can improve the connection between tissue and electrodes to reduce the interface resistance and treat the skin to reduce its electric resistance [56,57] or use internal electrodes to bypass the skin.

Previous studies using agarose gel as a interstitium phantom showed an increase in electromobility with increasing either pulse

duration or pulse magnitude [38,58]. These dependences were attributed to the sieving mechanism of the agarose fiber matrix and the necessity of the DNA molecule to be deformed to an extent before it was able to reptate through the matrix. It was expected that the collagen fibers of the ECM would have a similar effect on DNA transport in vivo. However, the in vivo findings reported here appeared to contradict these previous findings as they showed that the dependences of electromobility on pulse magnitude and pulse duration of the applied field were statistically insignificant. The pulse duration and pulse magnitude only affected the ranges of data within the same experimental groups (see Fig. 4).

As a possible explanation for the above observations, the magnitude of pDNA movement observed in the 100 V/cm applied field may represent the initial movement of the molecule from its post injection site to its first encounter with a physical obstacle (i.e., cell or ECM) in tissues. The applied field of 100 V/cm, which yielded intratumoral electric fields of 17.9 and 23.0 V/cm in 4T1 and B16.F10, respectively, may not have been sufficient to deform the pDNA to the extent necessary to pass through the pores in the interstitium. This mechanism of DNA transport has been demonstrated in an agarose gel [58], suggesting that pDNA electrophoresis is relatively unhindered over approximately 250 and 500 nm distances in 4T1 and B16.F10 tumors, respectively. When the magnitude of electric field was increased to 400 V/cm, the intratumoral fields were increased to 200 and 237 V/cm in 4T1 and B16.F10, respectively, which were likely to be sufficient to allow pDNA to pass through the pores in the interstitium. As a result, the distances of pDNA movement increased significantly with increasing the pulse duration in both tumors.

In summary, this study provides the first known, direct quantification of electric field-induced interstitial transport of pDNA in vivo in tumors. The results showed that the magnitude of the transport, induced by a sequence of ten electrophoretic pulses commonly used in electric field-mediated gene delivery, was insufficient for DNA to move macroscopically through tissues. However, the magnitude of the movement was significantly greater than that observed in the absence of an applied electric field. Induced transport at this magnitude may be critical for local movement of pDNA from the interstitial space to the transient pores in the plasma membrane of electropermeabilized cells. To induce greater macroscopic movement of pDNA, additional methods must be developed to overcome transport barriers in tumor interstitium.

Acknowlegments

This work was supported in part by a grant from the National Institutes of Health (NIH) (CA94019). JWH was supported in part by a NIH training grant for the Center for Biomolecular and Tissue Engineering at Duke University.

References

[1] Y. Boucher, L.T. Baxter, R.K. Jain, Interstitial pressure gradients in tissue-isolated and subcutaneous tumors: implications for therapy, Cancer Res. 50 (1990) 4478–4484.
[2] P.A. Netti, L.M. Hamberg, J.W. Babich, D. Kierstead, W. Graham, G.J. Hunter, G.L. Wolf, A. Fischman, Y. Boucher, R.K. Jain, Enhancement of fluid filtration across tumor vessels: implication for delivery of macromolecules, Proc. Natl. Acad. Sci. U. S. A. 96 (1999) 3137–3142.
[3] A. Pluen, Y. Boucher, S. Ramanujan, T.D. McKee, T. Gohongi, E. di Tomaso, E.B. Brown, Y. Izumi, R.B. Campbell, D.A. Berk, R.K. Jain, Role of tumor-host interactions in interstitial diffusion of macromolecules: cranial vs. subcutaneous tumors, Proc. Natl. Acad. Sci. U. S. A. 98 (2001) 4628–4633.
[4] E. Neumann, M. Schaefer-Ridder, Y. Wang, P.H. Hofschneider, Gene transfer into mouse lyoma cells by electroporation in high electric fields, EMBO J. 1 (1982) 841–845.
[5] H. Potter, Electroporation in biology: methods, applications, and instrumentation, Anal. Biochem. 174 (1988) 361–373.
[6] E. Neumann, Membrane electroporation and direct gene transfer, Bioelectrochem. Bioenerg. 28 (1992) 247–267.
[7] H. Wolf, M.P. Rols, E. Boldt, E. Neumann, J. Teissie, Control by pulse parameters of electric field-mediated gene transfer in mammalian cells, Biophys. J. 66 (1994) 524–531.
[8] E. Neumann, S. Kakorin, K. Toensing, Fundamentals of electroporative delivery of drugs and genes, Bioelectrochem. Bioenerg. 48 (1999) 3–16.
[9] L.M. Mir, M.F. Bureau, J. Gehl, R. Rangara, D. Rouy, J.M. Caillaud, P. Delaere, D. Branellec, B. Schwartz, D. Scherman, High-efficiency gene transfer into skeletal muscle mediated by electric pulses, Proc. Natl. Acad. Sci. U. S. A. 96 (1999) 4262–4267.
[10] L. Heller, M.J. Jaroszeski, D. Coppola, C. Pottinger, R. Gilbert, R. Heller, Electrically mediated plasmid DNA delivery to hepatocellular carcinomas in vivo, Gene Ther. 7 (2000) 826–829.
[11] J.M. Wells, L.H. Li, A. Sen, G.P. Jahreis, S.W. Hui, Electroporation-enhanced gene delivery in mammary tumors, Gene Ther. 7 (2000) 541–547.
[12] M. Bettan, M.A. Ivanov, L.M. Mir, F. Boissiere, P. Delaere, D. Scherman, Efficient DNA electrotransfer into tumors, Bioelectrochemistry 52 (2000) 83–90.
[13] F. Lohr, D.Y. Lo, D.A. Zaharoff, K. Hu, X. Zhang, Y. Li, Y. Zhao, M.W. Dewhirst, F. Yuan, C.Y. Li, Effective tumor therapy with plasmid-encoded cytokines combined with in vivo electroporation, Cancer Res. 61 (2001) 3281–3284.
[14] S. Li, Z. Ma, Nonviral gene therapy, Curr. Gene Ther. 1 (2001) 201–226.
[15] T. Tamura, T. Nishi, T. Goto, H. Takeshima, S.B. Dev, Y. Ushio, T. Sakata, Intratumoral delivery of interleukin 12 expression plasmids with in vivo electroporation is effective for colon and renal cancer, Hum. Gene Ther. 12 (2001) 1265–1276.
[16] M.L. Lucas, L. Heller, D. Coppola, R. Heller, IL-12 plasmid delivery by in vivo electroporation for the successful treatment of established subcutaneous B16, F10 melanoma, Mol. Ther. 5 (2002) 668–675.
[17] R. Heller, Delivery of plasmid DNA using in vivo electroporation, Preclinica 1 (2003) 198–208.
[18] F. Andre, L.M. Mir, DNA electrotransfer: its principles and an updated review of its therapeutic applications, Gene Ther. 11 (Suppl 1) (2004) S33–S42.
[19] M. Golzio, M.P. Rols, J. Teissie, In vitro and in vivo electric field-mediated permeabilization, gene transfer, and expression, Methods 33 (2004) 126–135.
[20] L.M. Mir, P.H. Moller, F. Andre, J. Gehl, Electric pulse-mediated gene delivery to various animal tissues, Adv. Genet. 54 (2005) 83–114.
[21] S. Kachi, Y. Oshima, N. Esumi, M. Kachi, B. Rogers, D.J. Zack, P.A. Campochiaro, Nonviral ocular gene transfer, Gene Ther. 12 (2005) 843–851.
[22] D.C. Chang, T.S. Reese, Changes in membrane structure induced by electroporation as revealed by rapid-freezing electron microscopy, Biophys. J. 58 (1990) 1–12.
[23] T.Y. Tsong, Electroporation of cell membranes, Biophys. J. 60 (1991) 297–306.
[24] D.C. Chang, Structure and dynamics of electric field-induced membrane pores as revealed by rapid-freezing electron microscopy, in: D.C. Chang, B.M. Chassy, J.A. Saunders, A.E. Sowers (Eds.), Guide to Electroporation and Electrofusion, Academic Press, Inc., San Diego, 1992, pp. 9–27.
[25] J.C. Weaver, Electroporation: a general phenomenon for manipulating cells and tissues, J. Cell. Biochem. 51 (1993) 426–435.
[26] R.F. Probstein, Physicochemical Hydrodynamics, John Wiley & Sons, Inc., New York, 1994.
[27] E. Neumann, S. Kakorin, K. Toensing, Principles of membrane electroporation and transport of macromolecules, in: M.J. Jaroszeski, R.

Heller, R. Gilbert (Eds.), Electrochemotherapy, electrogenetherapy, and transdermal drug delivery: Electrically mediated delivery of molecules to cells, Humana Press, Totowa, 2000, pp. 1–35.
[28] L.M. Mir, Therapeutic perspectives on in vivo cell electropermeabilization, Bioelectrochemistry 53 (2000) 1–10.
[29] P.J. Canatella, J.F. Karr, J.A. Petros, M.R. Prausnitz, Quantitative study of electroporation-mediated molecular uptake and cell viability, Biophys. J. 80 (2001) 755–764.
[30] J. Teissie, M. Golzio, M.P. Rols, Mechanisms of cell membrane electropermeabilization: a minireview of our present (lack of ?) knowledge, Biochim. Biophys. Acta 1724 (2005) 270–280.
[31] J.C. Weaver, Y.A. Chizmadzhev, Theory of electroporation: a review, Bioelectrochem. Bioenerg. 41 (1996) 135–160.
[32] J. Gehl, Electroporation: theory and methods, perspectives for drug delivery, gene therapy and research, Acta Physiol. Scand. 177 (2003) 437–447.
[33] E. Neumann, S. Kakorin, I. Tsoneva, B. Nikolova, T. Tomov, Calcium-mediated DNA adsorption to yeast cells and kinetics of cell transformation by electroporation, Biophys. J. 71 (1996) 868–877.
[34] M.F. Bureau, J. Gehl, V. Deleuze, L.M. Mir, D. Scherman, Importance of association between permeabilization and electrophoretic forces for intramuscular DNA electrotransfer, Biochim. Biophys. Acta 1474 (2000) 353–359.
[35] S. Satkauskas, M.F. Bureau, M. Puc, A. Mahfoudi, D. Scherman, D. Miklavcic, L.M. Mir, Mechanisms of in vivo DNA electrotransfer: respective contributions of cell electropermeabilization and DNA electrophoresis, Mol. Ther. 5 (2002) 133–140.
[36] S. Satkauskas, F. Andre, M.F. Bureau, D. Scherman, D. Miklavcic, L.M. Mir, Electrophoretic component of electric pulses determines the efficacy of in vivo DNA electrotransfer, Hum. Gene Ther. 16 (2005) 1194–1201.
[37] D.A. Zaharoff, R.C. Barr, C.Y. Li, F. Yuan, Electromobility of plasmid DNA in tumor tissues during electric field-mediated gene delivery, Gene Ther. 9 (2002) 1286–1290.
[38] D.A. Zaharoff, F. Yuan, Effects of pulse strength and pulse duration on in vitro DNA electromobility, Bioelectrochemistry 62 (2004) 37–45.
[39] P.A. Netti, D.A. Berk, M.A. Swartz, A.J. Grodzinsky, R.K. Jain, Role of extracellular matrix assembly in interstitial transport in solid tumors, Cancer Res. 60 (2000) 2497–2503.
[40] C.A. Edwards, W.D. O'Brien Jr., Modified assay for determination of hydroxyproline in a tissue hydrolyzate, Clin. Chim. Acta 104 (1980) 161–167.
[41] N. Pavselj, Z. Bregar, D. Cukjati, D. Batiuskaite, L.M. Mir, D. Miklavcic, The course of tissue permeabilization studied on a mathematical model of a subcutaneous tumor in small animals, IEEE Trans. Biomed. Eng. 52 (2005) 1373–1381.
[42] A. Leroy-Willig, M.F. Bureau, D. Scherman, P.G. Carlier, In vivo NMR imaging evaluation of efficiency and toxicity of gene electrotransfer in rat muscle, Gene Ther. 12 (2005) 1434–1443.
[43] P. Lefesvre, J. Attema, D. van Bekkum, A comparison of efficacy and toxicity between electroporation and adenoviral gene transfer, BMC Mol. Biol. 3 (2002) 12.
[44] X.Y. Zhang, J. Luck, M.W. Dewhirst, F. Yuan, Interstitial hydraulic conductivity in a fibrosarcoma, Am. J. Physiol. Heart Circ. Physiol. 279 (2000) H2726–H2734.
[45] Y. Wang, S. Liu, C.Y. Li, F. Yuan, A novel method for viral gene delivery in solid tumors, Cancer Res. 65 (2005) 7541–7545.
[46] S. McGuire, D. Zaharoff, F. Yuan, Nonlinear dependence of hydraulic conductivity on tissue deformation during intratumoral infusion, Ann. Biomed. Eng. 34 (2006) 1173–1181.
[47] M. Golzio, J. Teissie, M.P. Rols, Direct visualization at the single-cell level of electrically mediated gene delivery, Proc. Natl. Acad. Sci. U. S. A. 99 (2002) 1292–1297.
[48] Y. Antov, A. Barbul, H. Mantsur, R. Korenstein, Electroendocytosis: exposure of cells to pulsed low electric fields enhances adsorption and uptake of macromolecules, Biophys. J. 88 (2005) 2206–2223.
[49] E. Phez, C. Faurie, M. Golzio, J. Teissie, M.P. Rols, New insights in the visualization of membrane permeabilization and DNA/membrane interaction of cells submitted to electric pulses, Biochim. Biophys. Acta 1724 (2005) 248–254.
[50] F. Liu, S. Heston, L.M. Shollenberger, B. Sun, M. Mickle, M. Lovell, L. Huang, Mechanism of in vivo DNA transport into cells by electroporation: electrophoresis across the plasma membrane may not be involved, J. Gene Med. 8 (2006) 353–361.
[51] B.J. Mossop, R.C. Barr, J.W. Henshaw, D.A. Zaharoff, F. Yuan, Electric fields in tumors exposed to external voltage sources: implication for electric field-mediated drug and gene delivery, Ann. Biomed. Eng. 34 (2006) 1564–1572.
[52] S. Ramanujan, A. Pluen, T.D. McKee, E.B. Brown, Y. Boucher, R.K. Jain, Diffusion and convection in collagen gels: implications for transport in the tumor interstitium, Biophys. J. 83 (2002) 1650–1660.
[53] S.K. Hobbs, W.L. Monsky, F. Yuan, W.G. Roberts, L. Griffith, V.P. Torchilin, R.K. Jain, Regulation of transport pathways in tumor vessels: role of tumor type and microenvironment, Proc. Natl. Acad. Sci. U. S. A. 95 (1998) 4607–4612.
[54] D. Sel, S. Mazeres, J. Teissie, D. Miklavcic, Finite-element modeling of needle electrodes in tissue from the perspective of frequent model computation, IEEE Trans. Biomed. Eng. 50 (2003) 1221–1232.
[55] S.B. Dev, D. Dhar, W. Krassowska, Electric field of a six-needle array electrode used in drug and DNA delivery in vivo: analytical versus numerical solution, IEEE Trans. Biomed. Eng. 50 (2003) 1296–1300.
[56] M.R. Prausnitz, V.G. Bose, R. Langer, J.C. Weaver, Electroporation of mammalian skin: a mechanism to enhance transdermal drug delivery, Proc. Natl. Acad. Sci. U. S. A. 90 (1993) 10504–10508.
[57] J.C. Weaver, T.E. Vaughan, Y. Chizmadzhev, Theory of electrical creation of aqueous pathways across skin transport barriers, Adv. Drug Deliv. Rev. 35 (1999) 21–39.
[58] J.W. Henshaw, D.A. Zaharoff, B.J. Mossop, F. Yuan, A single molecule detection method for understanding mechanisms of electric field-mediated interstitial transport of genes, Bioelectrochemistry 69 (2006) 248–253.
[59] R.K. Jain, Barriers to drug delivery in solid tumors, Sci. Am. 271 (1994) 58–65.